

Pulsed Galvanostatic Synthesis of Zinc Oxide Nanostructures

Hassan Karami^{1,*}, Ziba Bigdeli², Sara Matini²

¹Department of Chemistry, Payame Noor University, Tehran, Iran

²Nano Research Laboratory, Department of Chemistry, Payame Noor University, Abhar, Iran

*E-mail: karami_h@yahoo.com

Received: 15 Nvember 2015 / Accepted: 13 February 2016 / Published: 1 March 2016

In the present paper, various nanostructures of zinc oxide are prepared by the pulse current electrochemical technique on the zinc substrate in sodium sulfide solution as a pH adjuster. To achieve homogenous morphology, smallest size distribution, and the best composition of sample, the impacts of experimental variables including sodium sulfide concentration, type and concentration of additives, pH, bath temperature, frequency and height of the pulse (current density) have been evaluated. The synthesized nanoparticles have been carefully characterized using several techniques such as scanning electron microscopy (SEM), transmission electron microscopy (TEM), energy dispersive X-ray analysis (EDX), and X-ray diffraction (XRD). The results revealed that the morphology and particle size of ZnO samples depends strongly on the amounts of synthesis parameters. The ZnO sample synthesized in 62.5 mA.cm^{-2} density of current, pulse and relaxation time of 1 s, mixing rate of 200 rpm, 0.001 M Na_2S , solution pH of 12.7, and electrocrystallization temperature of $45 \text{ }^\circ\text{C}$, 5 g/l PVP as manager of structure additive includes uniform ZnO nanoparticles with 30 nm average diameter. When the synthesis solution is at a standstill and the CMT is zero, ZnO sample includes uniform nanosheets with average thickness lower than 30 nm. According to the results, the pulsed galvanostatic technique can be used as a valid and controllable method to synthesize the zinc oxide nanoparticles.

Keywords: Zinc oxide, Nanoparticles, Electrosynthesis, Pulsed current, Electrocrystallization

1. INTRODUCTION

Nanomaterials in diverse fields of science and technology [1-2] have received increasing attention. Different physicochemical methods, such as metal evaporation [3], spray pyrolysis [4], sol-gel [5] and electrochemical techniques [6] have been applied to synthesize nanoscaled materials.

The electrochemical synthesis is a low cost method, the synthesis reaction can be performed under moderate conditions and the characteristics of nanoparticles can be controlled by several factors such as density of current, applied potential, temperature, and composition of the solution. Recently,

numerous nanostructures have been prepared by the electrochemical techniques like cyclic voltammetry [7-10], potentiostatic [11-15], galvanostatic [16-17], and pulsed-current [18-22] methods. Pulse galvanostatic method is an effective, simple, and controllable method. In the pulsed current, nanostructured materials can be synthesized on the electrode by controlling pulse variables including height of the pulse (current density), pulse and relaxation time. Many reports show that the pulsed-current electrosynthesis is more efficient than the direct current [23-26].

ZnO nanoparticles have gained much attention because of their unique catalytic, optical, gas sensing, and electrical features, and a significant excitation bonding energy. Good electrical, optical, and piezoelectric properties, non-toxicity, low cost and wide applications in various areas are some of the reasons for this remarkable attention about ZnO. More recently, attentions have been focused on the synthesis of nanostructured zinc oxide. Khorsand Zak et al. [27] synthesized hierarchical zinc oxide nanostructures via a simple sonochemical method. Zinc oxide nanostructures as single-crystalline were prepared by solvothermal method using methanol as solvent by Y. Yu et al. [28]. Zeng et al. [29] reported a new wet-chemical approach at 180 °C for the synthesis of monodispersed ZnO nanorods with high single-crystallinity. In a typical vapor-solid (VS) process, a mixture of zinc oxide nanostructures including nanohelices and nanobelts were synthesized by Kong et al. [30]. A simple procedure to obtain nanowires, nanoribbons and nanorods was reported by Yao et al. [31] which ZnO powder was mixed with graphite and heated to 1100 °C. After cooling, nanostructures were formed on the wall of the furnace. Karami [32] developed a sol-gel pyrolysis technique based on polymeric network of polyvinyl alcohol (PVA) to synthesis a novel CdO-ZnO nanocomposite. Bisio et al. [33] synthesized highly luminescent zinc oxide nanoparticles through a co-precipitation method, by start from a solution of zinc acetate in methanol and precipitating the oxide phase in alkaline environments in the presence of variable amounts of aminopropyl triethoxy silane (APTS). A novel dc thermal plasma reactor was applied to synthesize zinc oxide nanoparticles by Lin et al. [34]. In this project, we have used a pulse current technique for direct synthesis of zinc oxide nanoparticles in aqueous solution containing sodium sulfate as ionic strength adjuster, sodium sulfide as adjuster of pH and polyvinyl pyrrolidone (PVP) as manager of structure. Some experiments based on the "one at a time" method were performed to establish the optimal conditions for the synthesis of ZnO nanostructures with uniform morphology and narrowest size distribution.

2. EXPERIMENTAL

2.1. Materials

All reagents and chemicals were in analytical grade and purchased from Fluka, Merck, and Aldrich companies. Net lead substrate was bought from the National Iranian Lead-Zinc Company (NILZ Co., Zanjan, Iran). Double-distilled water was consumed in all tests.

2.2 Instrumentation

The particles size and morphology of zinc oxide samples were investigated by a Philips scanning electron microscopy method (XL30 model). Powder samples were analyzed by a XRD apparatus from Philips Co. (X Per) using the Cu (K_{α}) radiation and graphite monochromator. Energy dispersive X-ray analyses (EDX) were done by Philips 30 XL. X-ray diffraction (XRD) studies were accomplished by a Decker D8 instrument. The temperature of the synthesis solution was kept constant by water bath (Optima, Tokyo, Japan).

2.3. Methodology

2.3.1. Preparation of electrode

To preparation of zinc electrodes, pure zinc was melted in 420 °C and cast in a steel mould. The design and dimensions of the resultant electrode is illustrated in Fig.1.

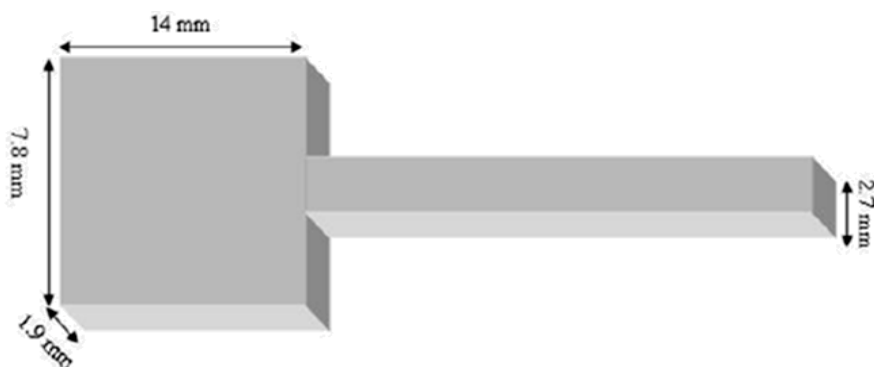


Figure 1. Design and dimensions of the casted zinc electrode

2.3.2. Zinc oxide synthesis

Before any electrodeposition, the zinc electrode was put in concentrated HNO_3 (65% w/w) for 30s and then was washed with double-distilled water to remove any surface oxidized impurities exposed to the air. Two graphite cathodes paired with given zinc anode electrode as an electrochemical cell. The electrodes were immersed in a synthesis solution containing 0.1 M sodium sulfate, 0.001 M sodium sulfide as pH controller ($\text{pH} = 12.7$), the electrocrystallization temperature of 45 ° C, 5 g/L PVP as manager of the structure additive. Various pulse current rates were served to reducing the Zn^{2+} ions on the cathode surface. The effects of all the factors, including pH, concentration of Na_2S , type and concentration of additive, temperature of the solution, and amplitude of the pulse current was optimized by "one at a time" method.

3. RESULTS AND DISCUSSION

3.1. Pulses characterisations

Nanoparticles of zinc oxide were directly prepared by the pulse current technique on stainless steel electrode in synthesis solution including 0.1 M sodium sulfate, 0.001 M sodium sulfide, solution pH of 12.7, electrocrystallization temperature of 45 °C, 5 g/l PVP as the manager of structure additive. In the present study, a direct current with fixed amplitude was provided by common power supply tools. The output of the power supply system (DC current) was linked to a home-made pulse maker device. As it can be seen in Fig. 2, the current output of the pulse system is a pulsed direct current.

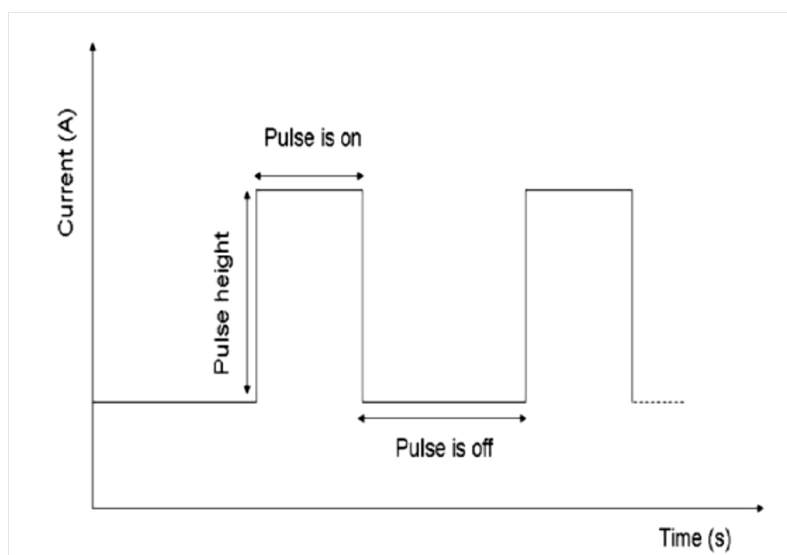


Figure 2. The pulse current chart containing the pulse and relaxation times and height of the pulse.

By considering Fig. 2, there are four various factors in a pulse galvanostatic method including height of the pulse (current density), pulse time (t_{on}), relaxation time (t_{off}) and frequency of the pulse. The results of previous studies confirmed the compliance of t_{off}/t_{on} ratio of 3 for most syntheses. Therefore, this ratio was used in further studies and, the other parameters includes the height of the pulse, pulse time and its frequency were kept constant.

3.2. Effect of the current amplitude

The height of the pulse impact (current amplitude) was explored on the morphology and particle sizes of the prepared zinc oxide nanoparticles. The height of the pulse was changed from 6.25 mA.cm⁻² to 125 mA.cm⁻², and the other parameters were kept fixed (temperature of 45 °C, 0.001 M sodium sulfide and pH 12.7). The particles size and morphology of the synthesized zinc oxide samples were investigated by SEM technique. Figure 3 illustrates the SEM images of the resultant zinc oxide samples in various the amplitude of pulsed current.

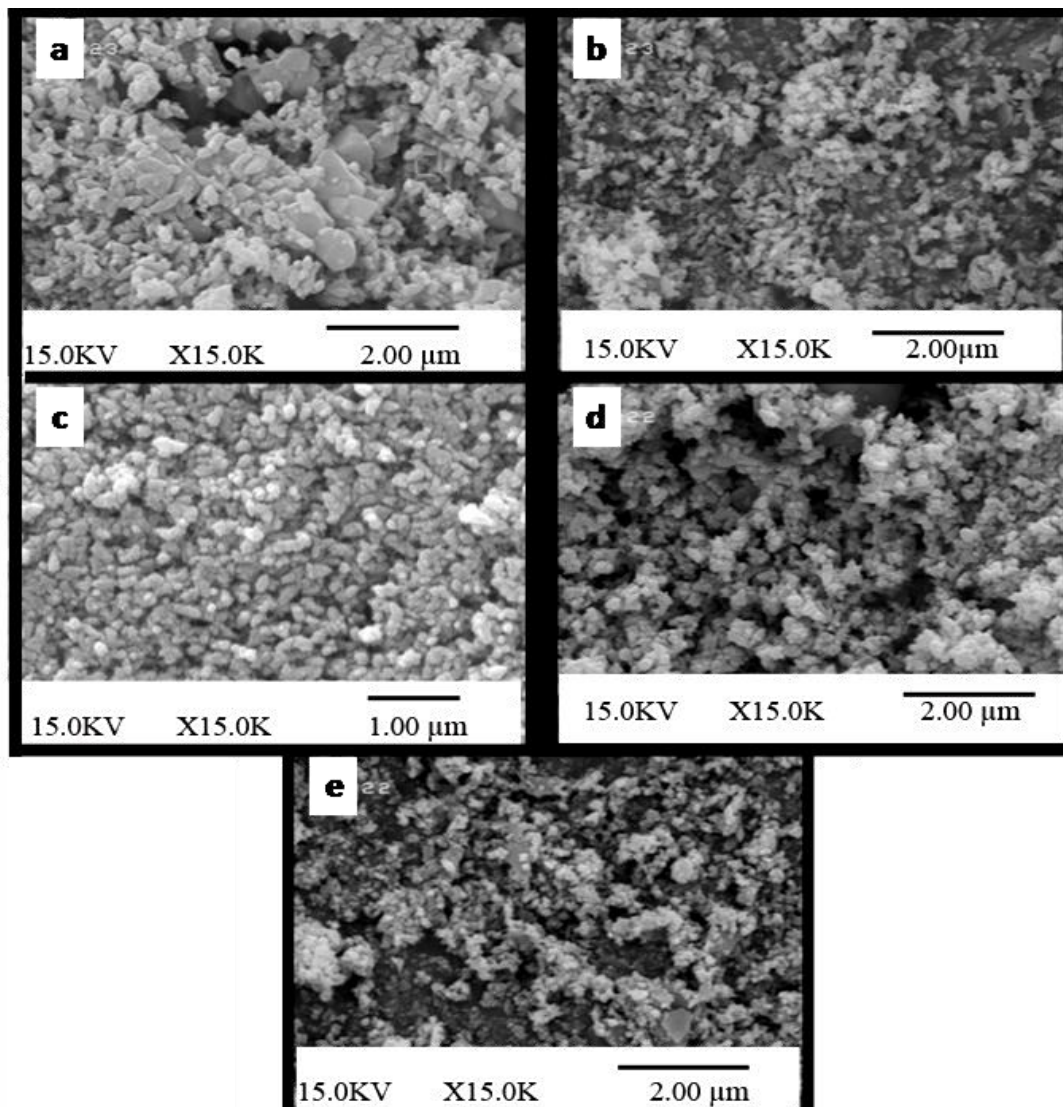


Figure 3. The images of zinc oxide examples for SEM which synthesized in various pulsed current amplitudes; 6.25 mA.cm^{-2} (a), 18.75 mA.cm^{-2} (b), 31.25 mA.cm^{-2} (c), 62.5 mA.cm^{-2} (d) and 125 mA.cm^{-2} (e). The other experimental parameters were kept fixed.

It can be found in Fig. 3, the height of 62.5 mA.cm^{-2} for pulse creates more fine and homogenous nanoparticles than the others. At lower heights of pulse, greater and agglomerated particles have been synthesized because, in low pulse current, the nucleation speed is slower than the rate of particle growth. The pulse heights more than 62.5 mA.cm^{-2} create a high synthesis rate, thus the synthesized zinc oxide sample is not homogeneous (Fig. 3e).

3.3. Effect of synthesis temperature

Among the synthesis factors, the temperature of the solution had more influence on phase composition of the prepared zinc oxide examples. So, five samples were produced in various temperatures. The prepared samples were identified by SEM technique. Figure 4 indicates the images

of zinc oxide examples for SEM that prepared at 0, 25, 45, 70 and 90 °C. When the electrosynthesis was implemented at temperatures lower than 45 °C, the speed of reaction was very slow and the synthesized nanoparticles were smaller but not uniform. At higher temperatures, the reaction rate is high, but the prepared examples also show more agglomeration and non-uniform morphology.

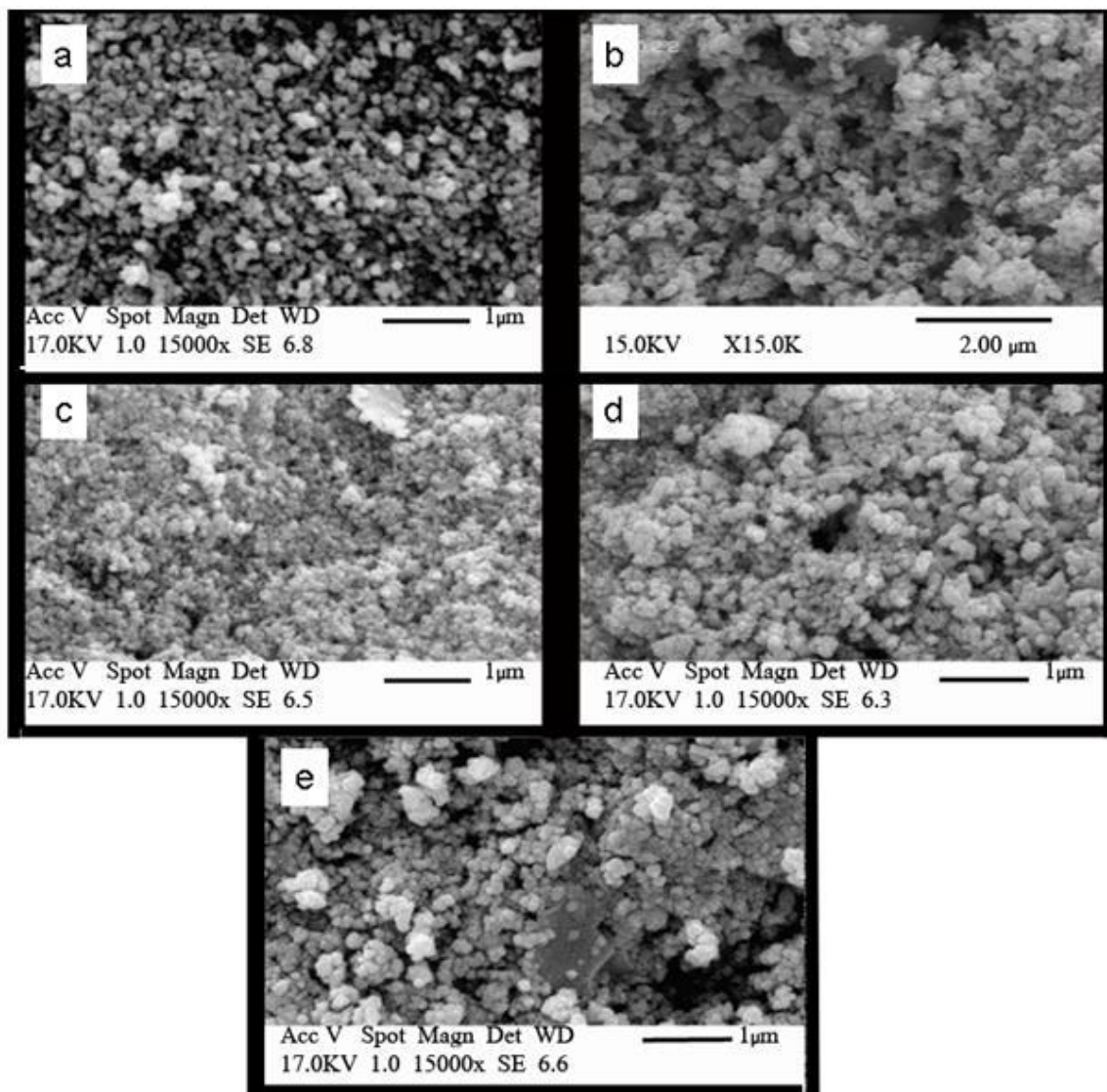


Figure 4. The images of zinc oxide examples for SEM that synthesized at temperatures of 0 °C (a), 25 °C (b), 45 °C (c) 70 °C (d) and 90 °C (e); the other parameters were kept fixed.

The examples synthesized at 0, 25, 45, 70 and 90 °C were also analyzed by X-ray diffraction technique. Figure 5 illustrates the patterns of XRD for these examples. It is obvious in Fig. 5 that temperature of the solution plays an important role in phase control and composition of the sample. At temperatures lower than 45 °C, zinc sulfide and zinc hydroxide can be synthesized, but at 45 °C and higher temperature, the sample will be consist of pure ZnO. By mixing the SEM and XRD results with regards to temperature studies confirms that the zinc oxide example synthesized at 45 °C has homogenous morphology, small particles slight amounts of impurities.

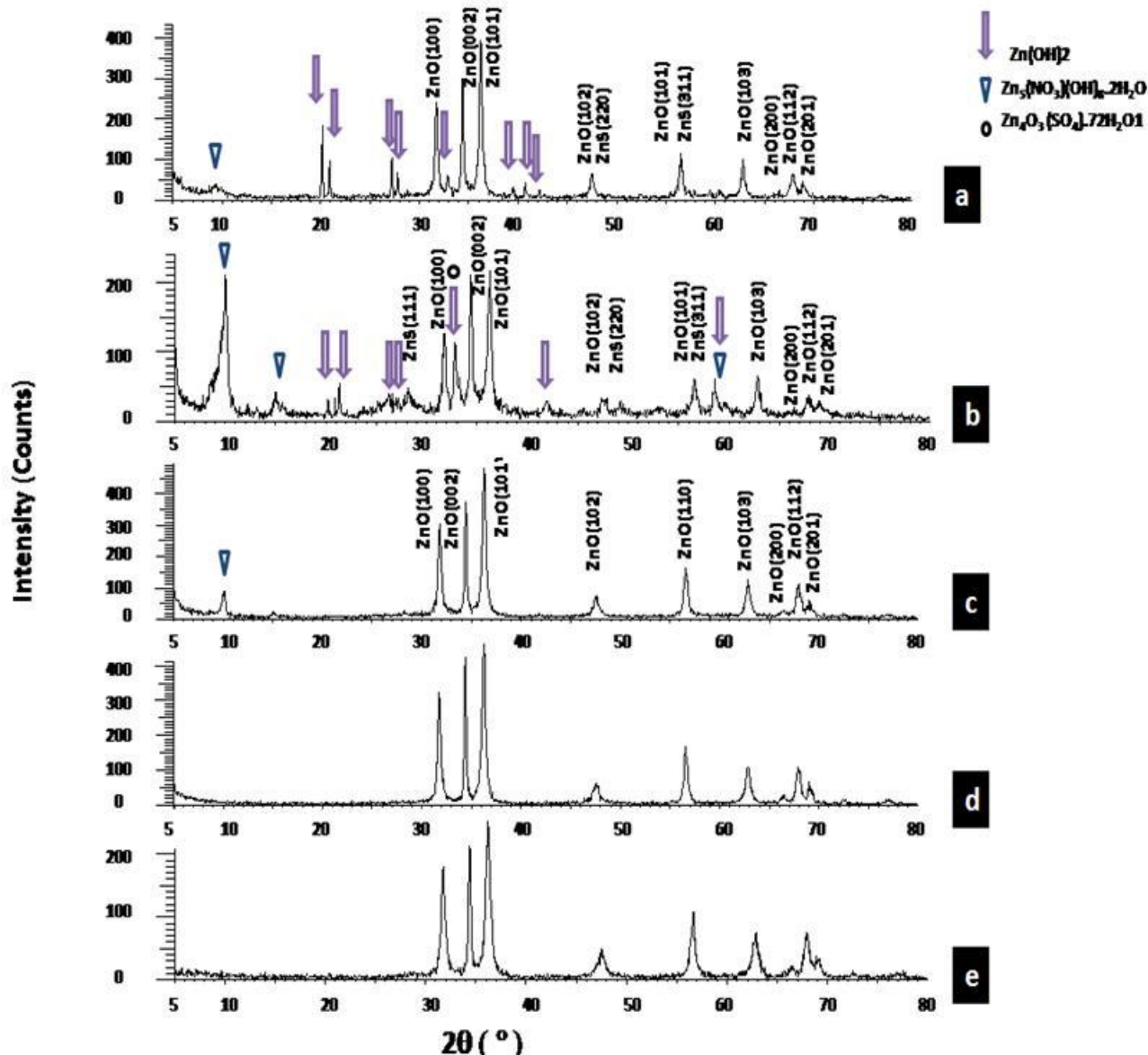
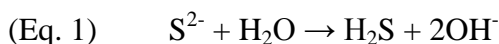


Figure 5. The patterns of XRD for the ZnO examples that synthesized in various temperatures of 0 °C (a), 25 °C (b), 45 °C (c) 70 °C (d) and 90 °C (e).

3.4. Effect of solution pH

In the proposed method, zinc ions are produced by direct anodic oxidizing of zinc electrode. The produced Zn^{2+} ions coupled with hydroxide ions to form $Zn(OH)_2$. Finally, zinc hydroxide is thermally decomposed and converted to ZnO. If the synthesis solution, sulfide ions reacts with water molecules and converted to hydrogen sulfide and hydroxide ions. The mentioned reactions for the preparation of ZnO are as follows:



The reaction between water and sulfide ions is strongly depends on solution pH. However, it is expected that the pH of experimental solution is an important factor with regard to the zinc oxide electrocrystallization. To achieve this propose, five examples synthesized at pHs of 7, 10.5, 11, 12.7 and 14. Figure 6 indicates the images of ZnO examples for SEM. The results show that the pH of 12.7 is appropriate to synthesize homogenous ZnO nanoparticles. The sample was agglomerated significantly, at lower pHs. The sample prepared at pH of 14 consisting the agglomerated and non uniform nanoparticles.

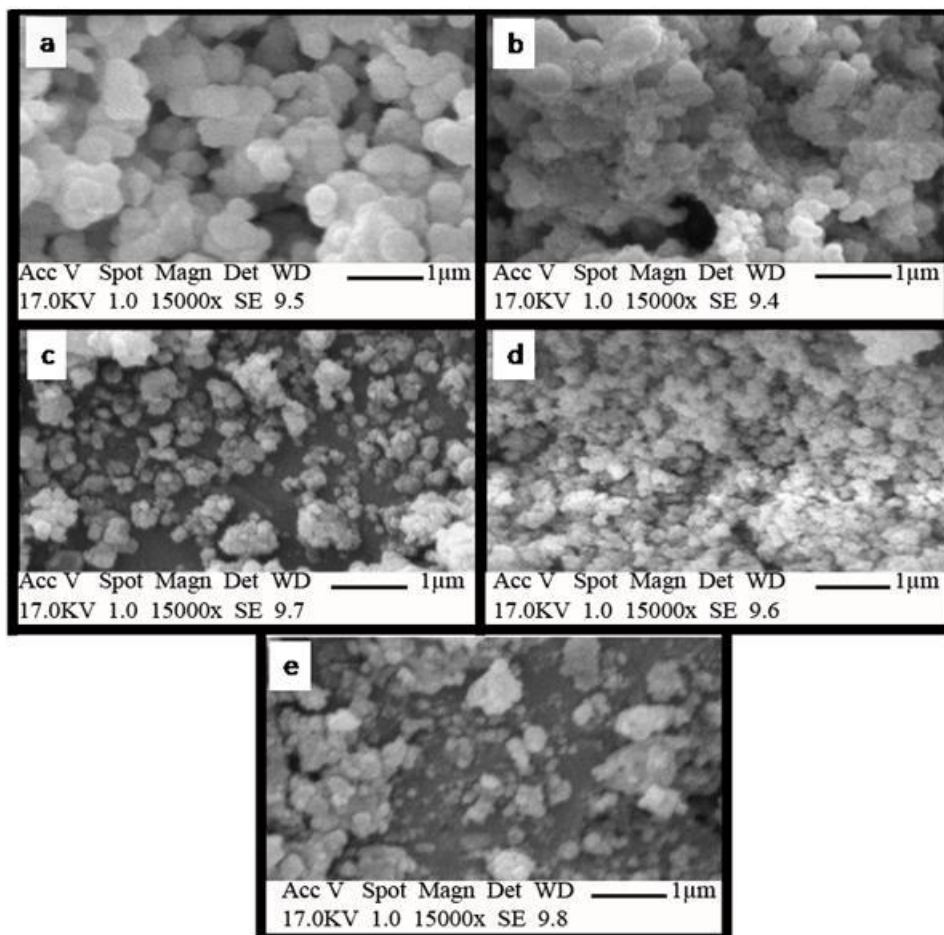


Figure 6. The images of ZnO examples for SEM that synthesized at various pHs 7 (a), 10.5 (b), 11 (c) 12.7(d) and 14 (e).

3.5. Optimizing the concentration of sodium sulfide

The substance of sodium sulfide is used as subsidiary electrolyte and pH adjuster. To examine the effect of this chemical's concentration on the particle size and morphology, the amount of this parameter was changed from 0.0001 to 1 M while the other parameters were kept fixed. Figure 7 illustrates the images of ZnO examples for SEM that synthesized in various concentrations of sodium sulfide.

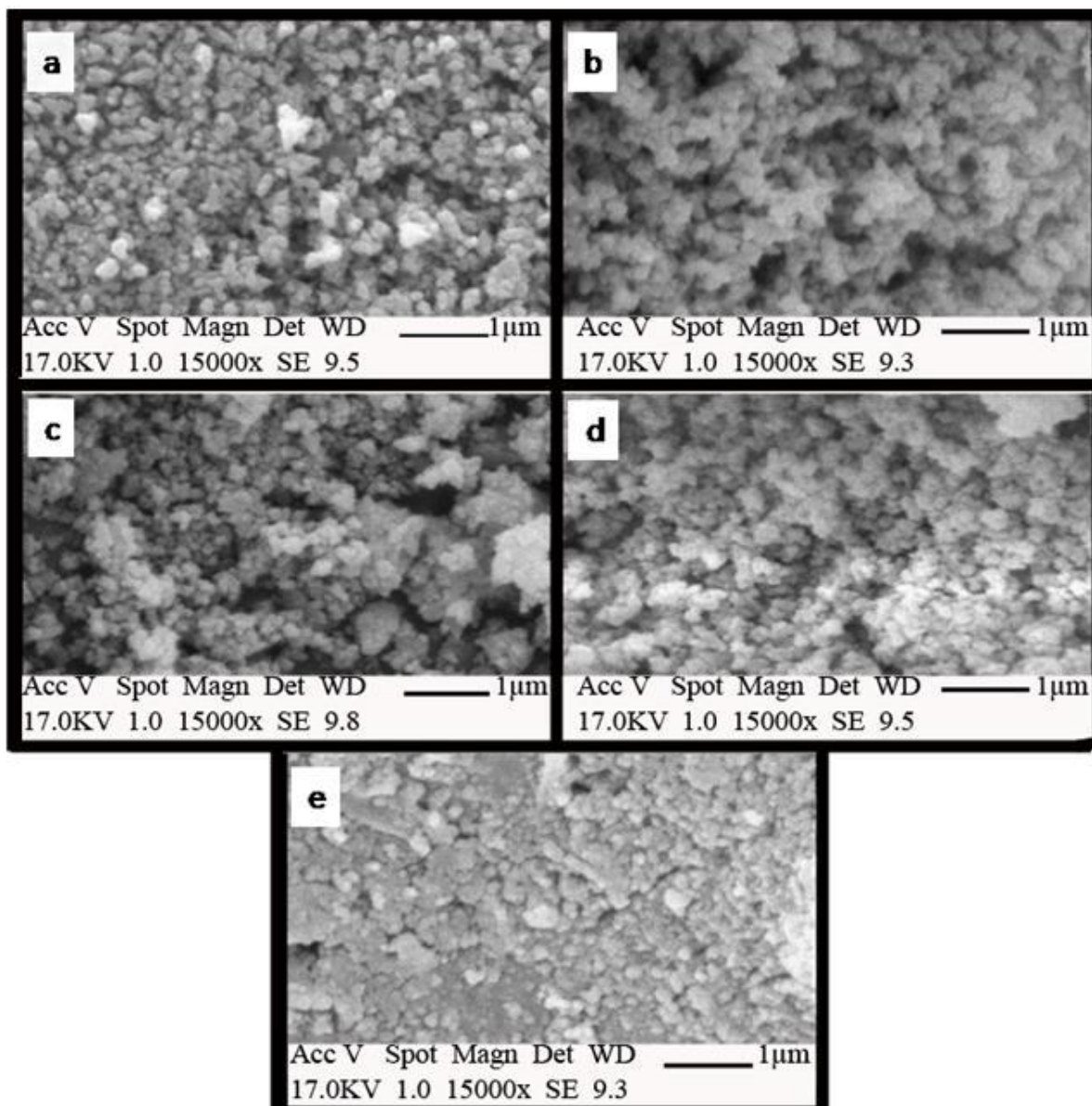


Figure 7. The images of ZnO examples for SEM which synthesized at sodium sulfide concentrations of 0.0001 M (a), 0.001 M (b), 0.01 M (c), 0.05 M (d), and 1 M (e).

The SEM images in Fig. 7 shows that in 0.001 M concentration of sodium sulfide, zinc oxide nanoparticles will be smaller as well as uniform morphology and in higher concentrations, agglomeration of the sample will be seen. So, this concentration of sodium sulfide can be used as optimal value.

3.6. Impact of additive synthesis

On the basis of the previous reports, some compounds like sodium dodecyl sulfate (SDS), cetyltrimethyl ammonium bromide (CTAB), glycerol, saccharin, polyvinyl pyrrolidone (PVP) as the manager of structure to achieve more uniform nanostructures. Preliminary studies indicated that SDS

and PVP are appropriate for electrocrystallization of zinc oxide nanoparticles in basic environments. Figure 8 shows the impact of various concentrations of PVP and SDS on the particles size and morphology of ZnO. The results confirmed that PVP are more effective to achieve more fine and uniform zinc oxide nanoparticles than SDS. However, as Fig. 8 shows, uniform zinc oxide nanoparticles without any agglomeration is available at 5 g/l PVP as optimal amount (Fig. 8b). Zinc ions can react with PVP to form a stable complex. The PVP complex can control the kinetics of ZnO formation.

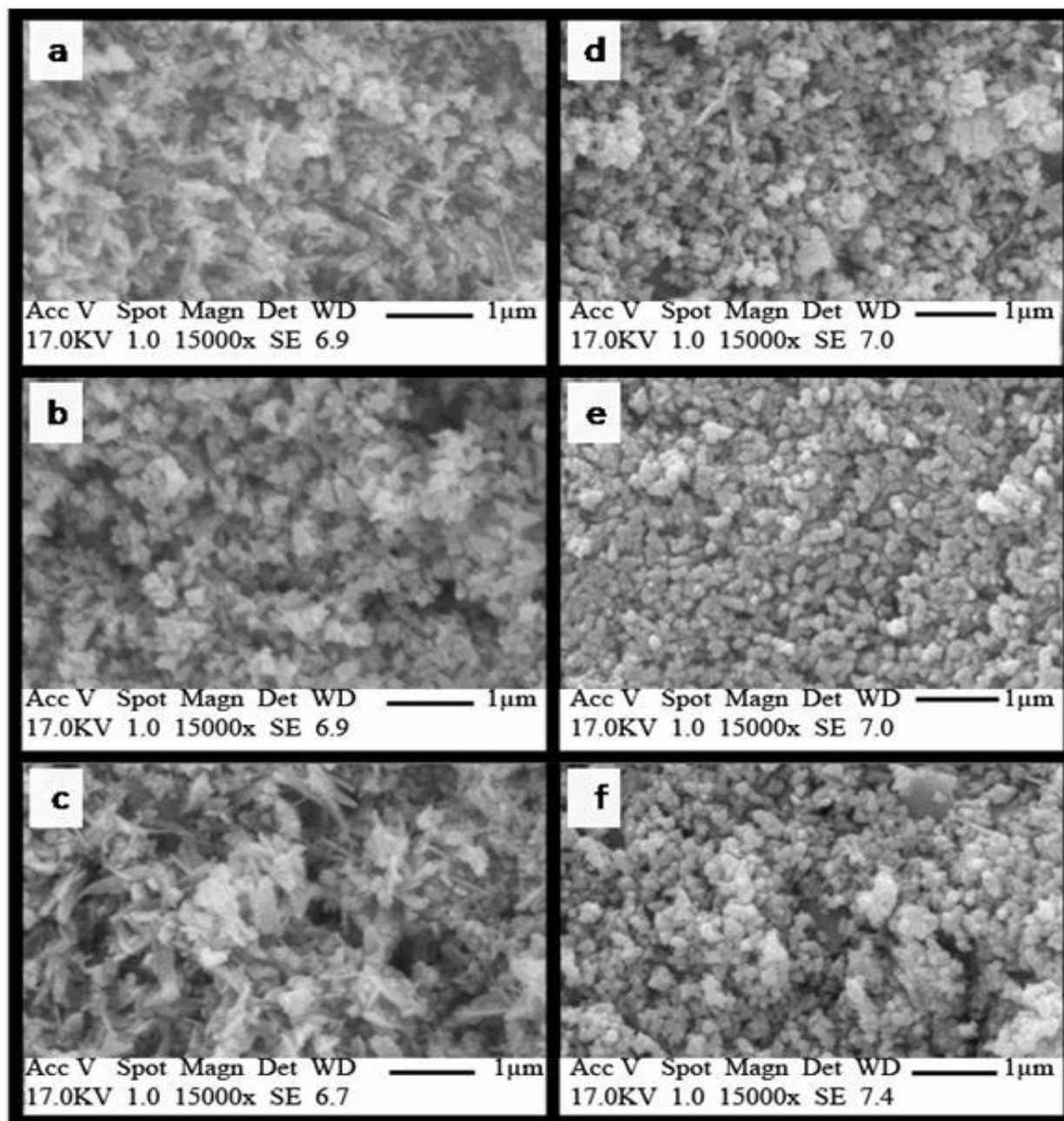


Figure 8. The images of ZnO examples for SEM which synthesized in the presence of 1 g.L⁻¹ PVP (a), 5 g.L⁻¹ PVP (b), 20 g.L⁻¹ PVP(c), 1 g.L⁻¹ SDS (d), 5 g.L⁻¹ SDS (e), 20 g.L⁻¹ SDS (f).

3.7. Effect of pulse on

In this section, the effect of t_{on} was evaluated in terms of the morphology and particle size of ZnO examples. In these experiments, the amounts of other parameters were kept fixed (current density: $62.5\text{mA}\cdot\text{cm}^{-2}$, pH: 12.7, sodium sulfate concentration: 0.1M, sodium sulfide: 0.001M, PVP: $5\text{ g}\cdot\text{L}^{-1}$, temperature: $25\text{ }^\circ\text{C}$, mixing rate: 200 rpm and t_{off} : 1 s). Figure 9 shows the images of ZnO examples for SEM in various pulse times.

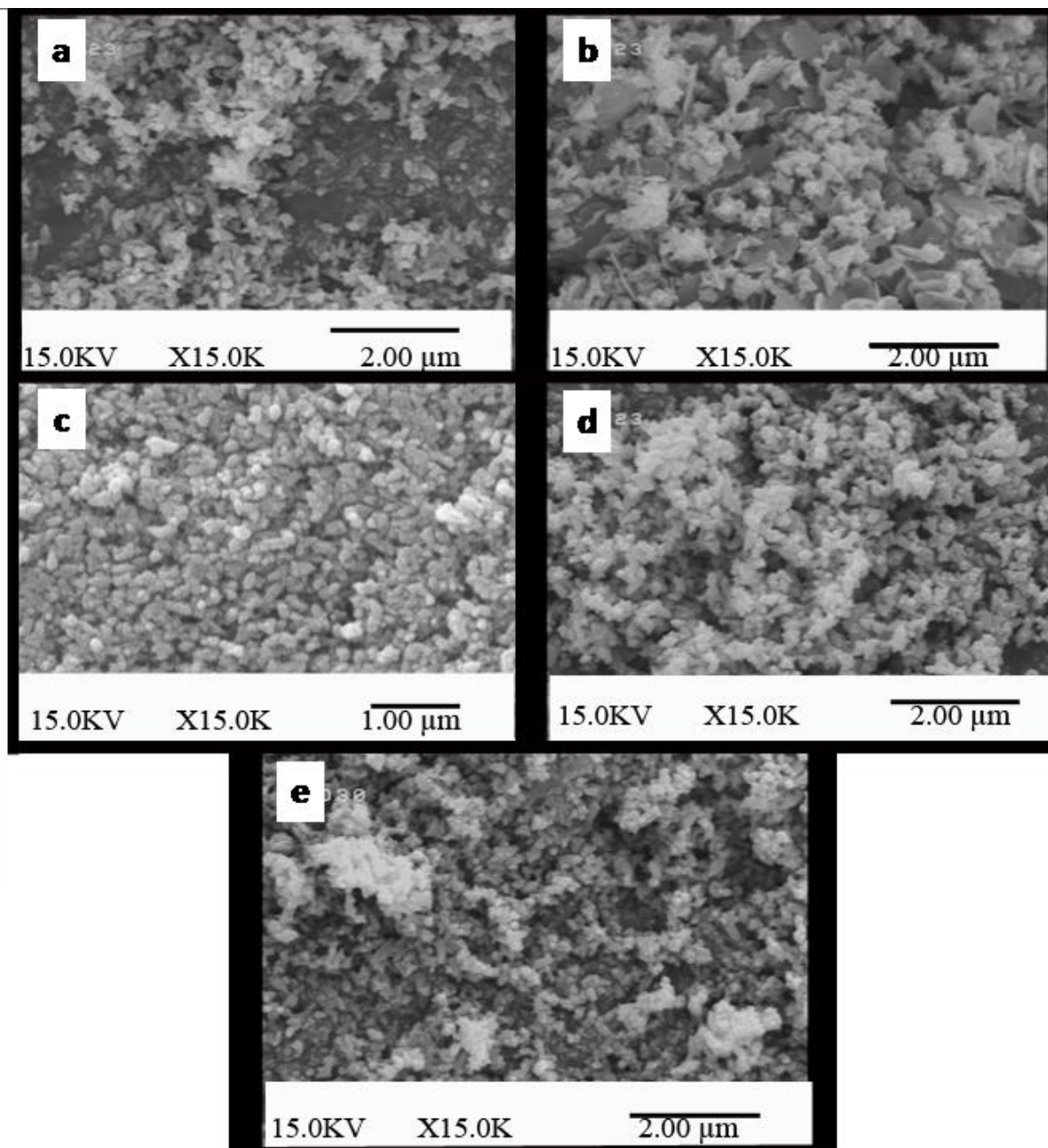


Figure 9. The images of ZnO examples for SEM that synthesized in various times of the pulse; 0.25 (a), 0.5 (b), 1 (c), 2 (d) and 3 s (e).

As can be seen in Fig. 9, at pulse time of 0.25 s, the particles are synthesized without any specific morphology. At pulse time of 0.5 s, the particles become larger without uniform morphology and nanoplates begin to form. As we can see at pulse time of 1 s (Fig. 9c), the sample contains the smallest uniform nanoparticles. In pulse time of 2 s, the particles size and agglomeration increase somewhat. In the last pulse time, as it can be seen in Fig. 9f, the fine particles without uniform morphology are dispersed among the agglomerated particles. It can be concluded that by increasing pulse time due to changes in the mechanism of synthesis, more regular particles with better morphology are synthesized. However, in terms of particle size and morphology, pulse time of 1 s was selected as the optimal value.

3.8. Optimization of relaxation time

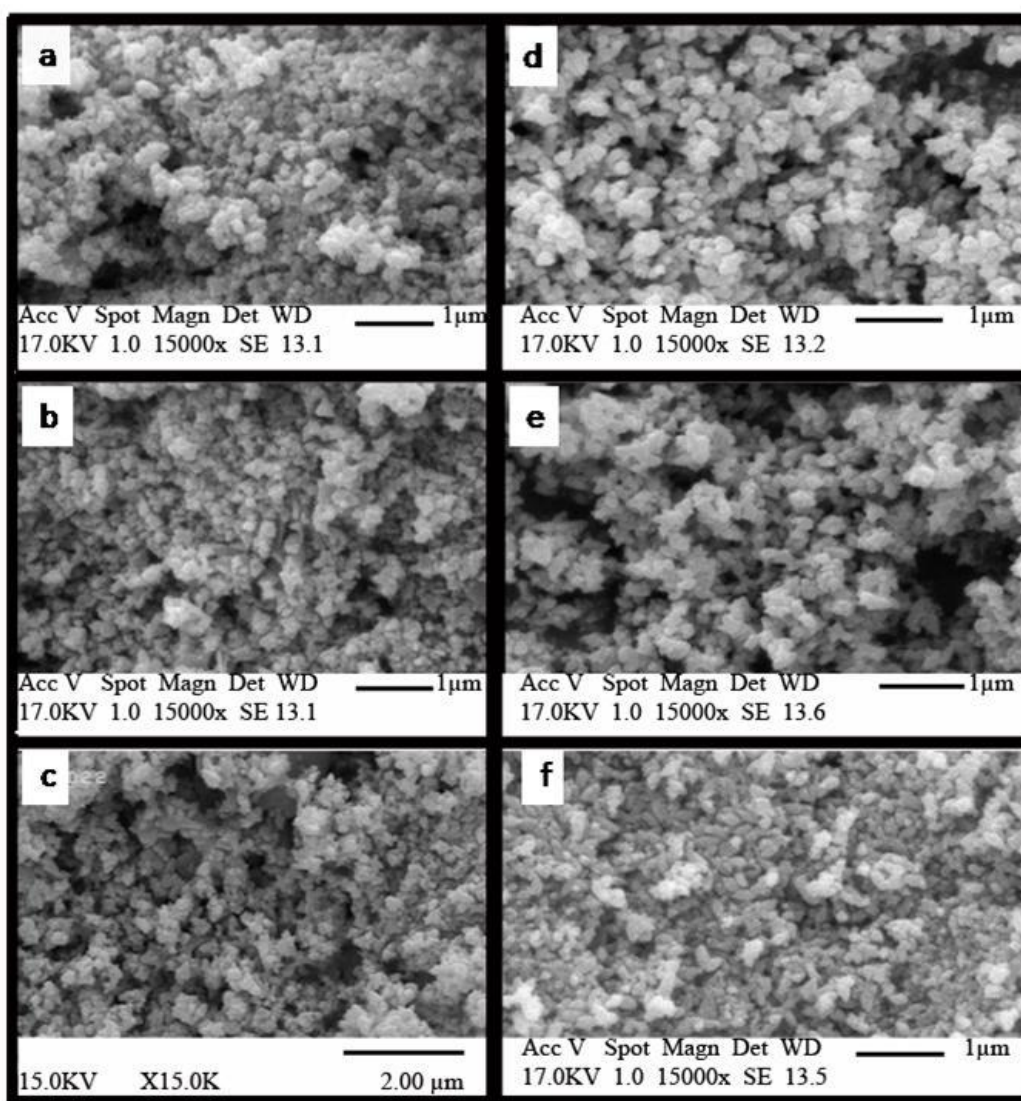


Figure 10. The images of ZnO examples for SEM that synthesized in various pulse times; 0 sec (a), 0.5 s (b), 1 s (c), 2 s (d) 3 s (e), and 4 s (f). Pulse time of 0 s is simple galvanostatic method (without pulse).

To study the relaxation time effect, six syntheses were performed as the preceding parameters were kept constant. Figure 10 shows the images of ZnO examples for SEM that synthesized in various relaxation times. As we can see in Fig. 10a, by using simple DC current (without pulse), ZnO particles are large and they are attached together to formation of lumps. At relaxation time 0.5 s, the ZnO particles become smaller and more uniform. At relaxation time of 1 s (Fig 10c), the ZnO sample containing smaller nanoparticles with better morphology than $t_{\text{off}} = 0.5$ s. By applying the longer t_{off} (Fig. 10d), in spite of more uniform morphology, the particles are larger and lump. At pulse time of 3 s, particles are agglomerated without uniform morphology. As can be seen in Fig. 10f, at pulse time of 4 s, in spite of regular morphology, there is high adhesion between particles and some lumps can be seen in the sample. Therefore, 1 s was chosen optimal value for the pulse time.

3.9. Optimizing the stirring rate of solution

Stirring (mixing) rate of the synthesis solution will be one of the effective factors on the morphology. To investigate the impact of this parameter, three examples prepared in various mixing rates as the other parameters were kept constant. The synthesized samples were identified by SEM.

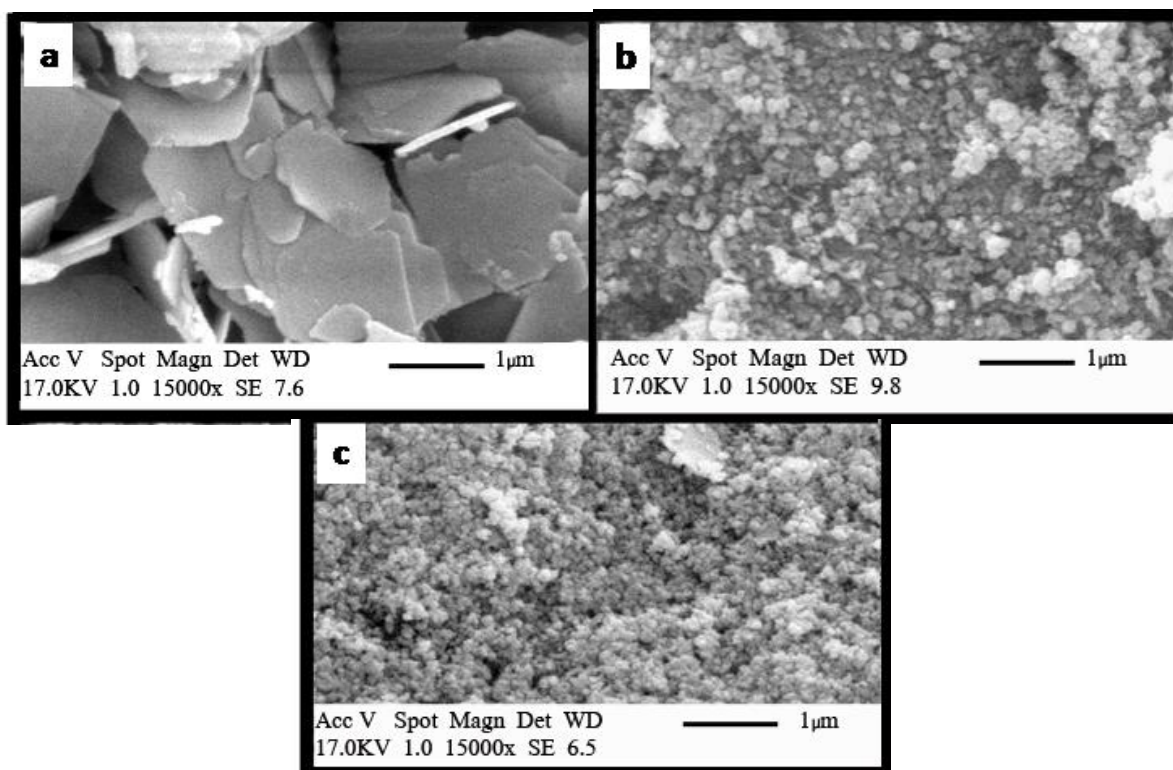


Figure 11. SEM images of ZnO prepared samples in different mixing rates of the synthesis solution; static solution: 0 $\frac{\text{rate}}{\text{min}}$ (a), 100 rpm (b), and 200 rpm (c).

Figure 11 indicates the SEM images of ZnO prepared samples at 0, 100, and 200 rpm. It can be seen, increasing mixing rate of the solution causes to change the uniform nanosheets (with average

thickness lower than 30 nm) to uniform nanoparticles (with average diameter lower than 30 nm). In this synthesis method, there are two types of mass transfers including diffusion mass transfer (DMT) and convection mass transfer (CMT). The mechanism of the synthesis depends strongly on the DMT and CMT rates. During electrosynthesis process, the DMT rate is same. Therefore, the observed differences between various morphologies of zinc oxide samples are relevant to CMT differences. Nanosheets' formation is performed with two dimensional growth while, the nanoparticles have similar growth in three dimensions. Two-dimensional growth needs a low rate of mass transfer. In the absence of CMT, DMT make this propose (the sample synthesized without stirring), because DMT is carried out only in vertical direction with respect to the anode surface (Fick's first law in mass transfer). By adding CMT to DMT cause to increase the mass transfer rate and disturb two-dimensional growth. By increasing the CMT rate, the growth rate in three dimensions will be similar so the nanoparticles are formed.

3.10. Characterization of the optimized ZnO sample

To distinction of the structure and characteristics of ZnO nanoparticle in optimum terms, it was determined by EDX and TEM. Figure 12 indicates TEM images of zinc oxide nanoparticles. Based on SEM and TEM images in the optimized conditions, the sample consisting uniform ZnO nanoparticles with 30 nm average diameters.

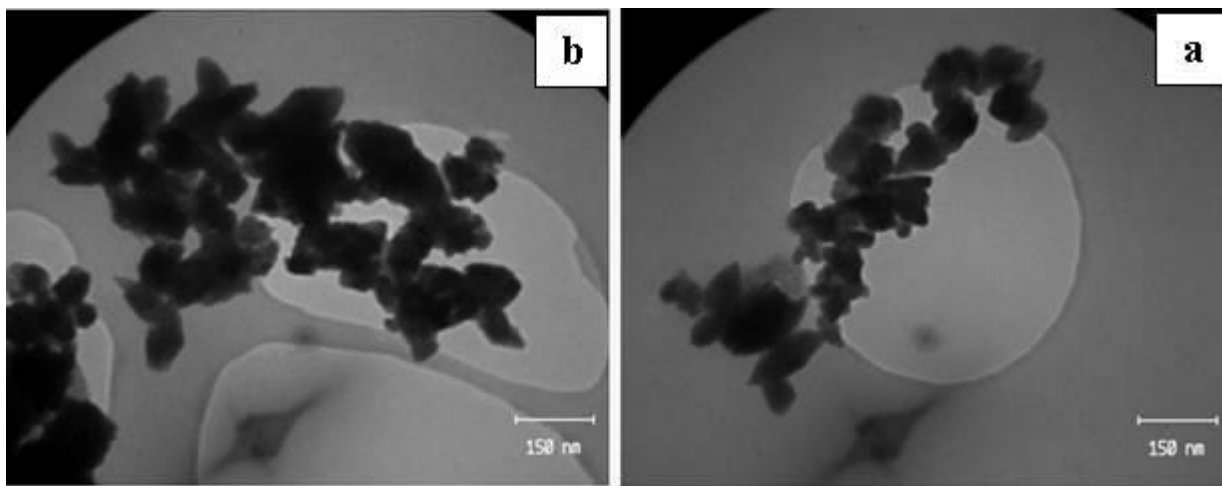


Figure 12. TEM sample images that are optimized in terms of synthesis. The sample has been synthesized in $62.5 \text{ mA}\cdot\text{cm}^{-2}$ current density, mixing rate of 200 rpm, 0.001 M Na_2S , temperature of electrocrystallization of 45°C , pH of 12.7 and electro- 45°C , and 5 g/L PVP as the structure manager add-on.

Zinc oxide sample was analyzed by EDX patterns (Fig. 13). The results indicate that the synthesized sample contains just zinc and oxygen elements.

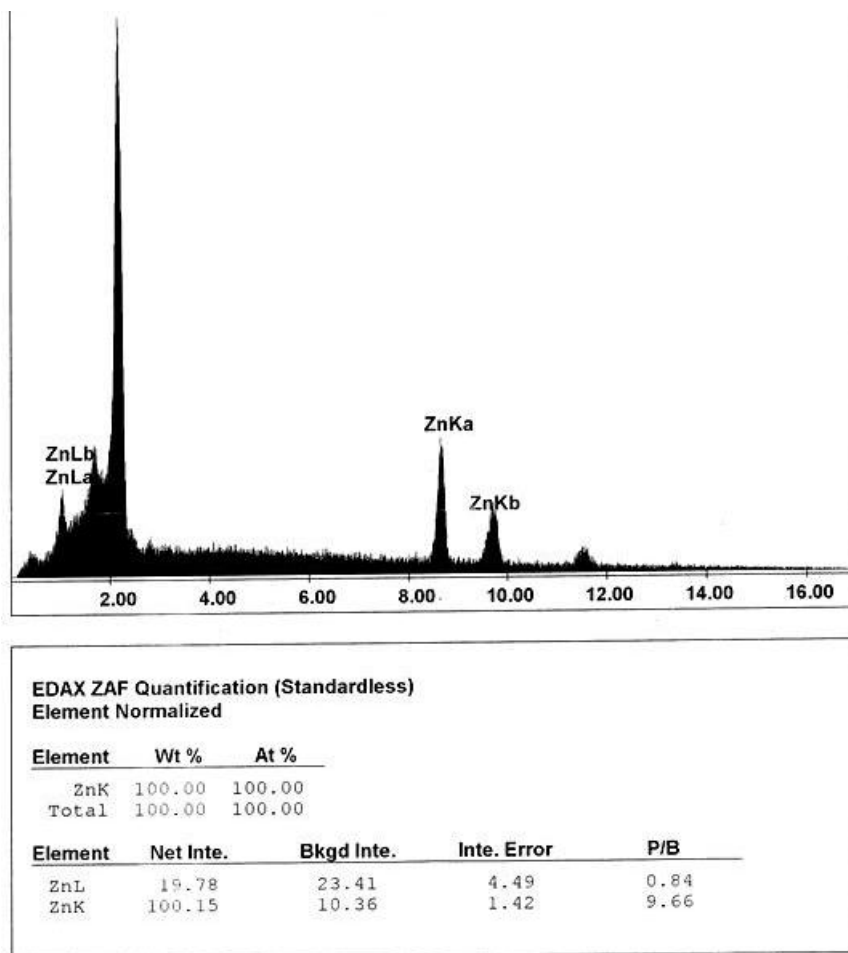


Figure 13. EDX patterns for ZnO sample which synthesized in the optimum conditions ($62.5 \text{ mA}\cdot\text{cm}^{-2}$ current density, rotation rate of 200 rpm, 0.001 M Na_2S , solution pH of 12.7, temperature of $45 \text{ }^\circ\text{C}$, 5 g/l PVP, without ultrasonic irradiation.)

3.11. The effect of morphology on the light absorbance

To examine the morphology of nanostructures’ effect on the absorption spectrum, five different ZnO examples were synthesized in different circumstances in accordance with Table 1.

Table 1. Empirical conditions for zinc oxide nanostructures synthesis in various morphologies.

Sample	Sodium sulfide (M)	pH	Current amplitude ($\text{mA}\cdot\text{cm}^{-2}$)	$t_{\text{on}}: t_{\text{off}}$ (s)	Additive ($\text{g}\cdot\text{l}^{-1}$)	Solution temperature ($^\circ\text{C}$)	Mixing rate of solution (rpm)
a	0.001	12.7	62.5	1: 1	PVP, 5	45	200
b	0.001	12.7	62.5	1: 1	PVP, 5	45	0
c	0.0001	1	31.25	1: 1	---	25	200
d	0.001	7.12	31.25	1: 1	SDS, 20	25	200
e	0.001	12.7	62.5	1: 1	PVP, 5	25	0

The selected samples were analyzed by SEM (Fig. 14). According to Fig. 14, the selected samples are quite different morphologies. To explore absorption spectra in chosen samples, then 0.2 g of each sample was dispersed in 5 ml of acetone. The spectrum of homogeneous suspension was seen within 200-600 nm. Figure 15 indicates the Uv-Visible spectra of the samples. So, a gap of energy in the samples will be counted by:

$$(Eq. 4) \quad E = \frac{hc}{\lambda}$$

Where, E (eV) is a gap of energy, h (6.63×10^{-34} J.s) is Planck's constant, c (3×10^8 m s⁻¹) is the speed of light and λ (nm) is the symbol of wavelength. The calculated data were listed in Table. By considering Table 2, the value of absorption wavelength and the gap of energy are close together in samples. For semiconductors, reducing the gap of energy, increases the electrical conductivity of the sample.

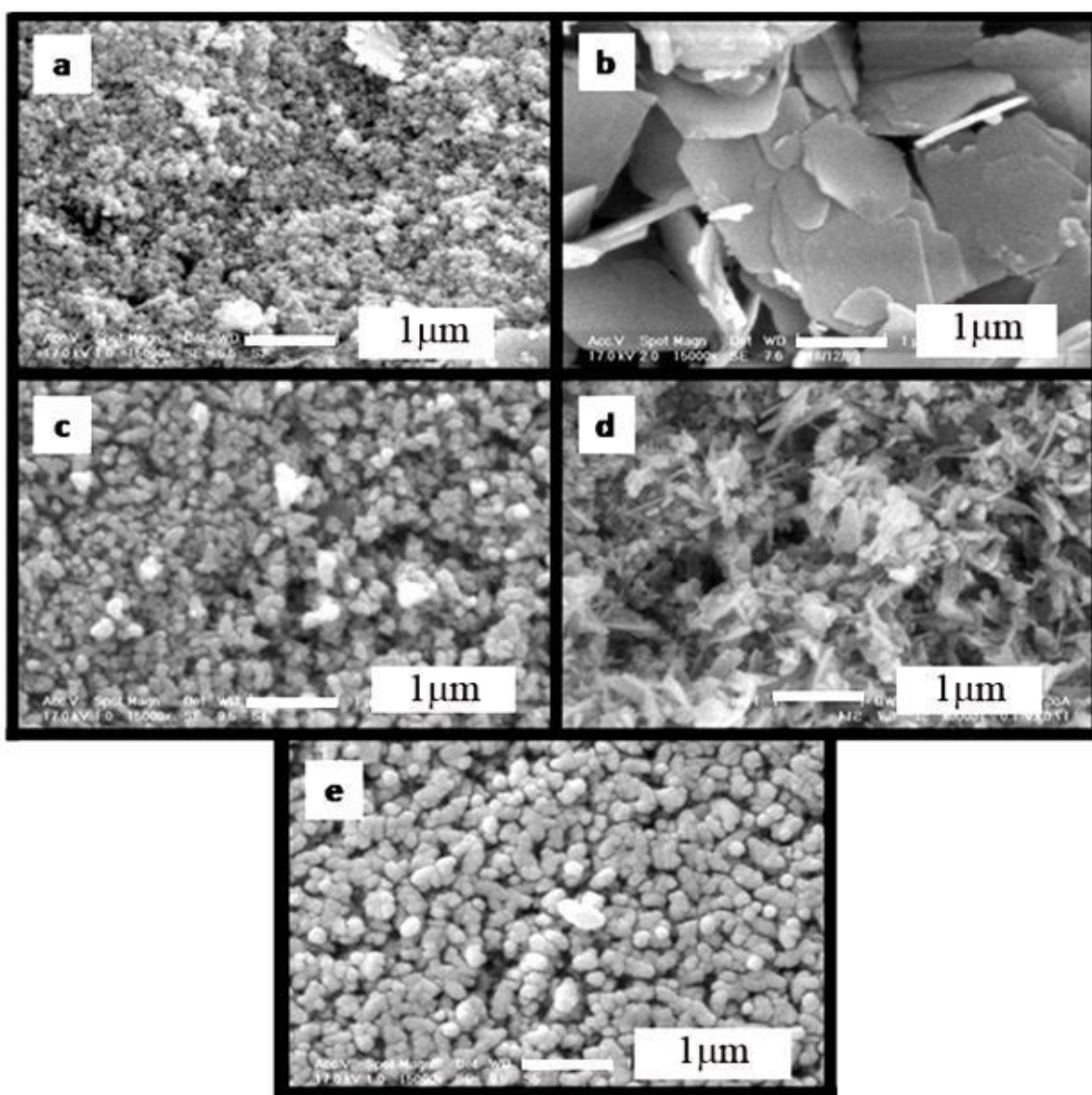


Figure 14. SEM pictures of the five samples were synthesized in various experimental circumstances, by considering Table 1.

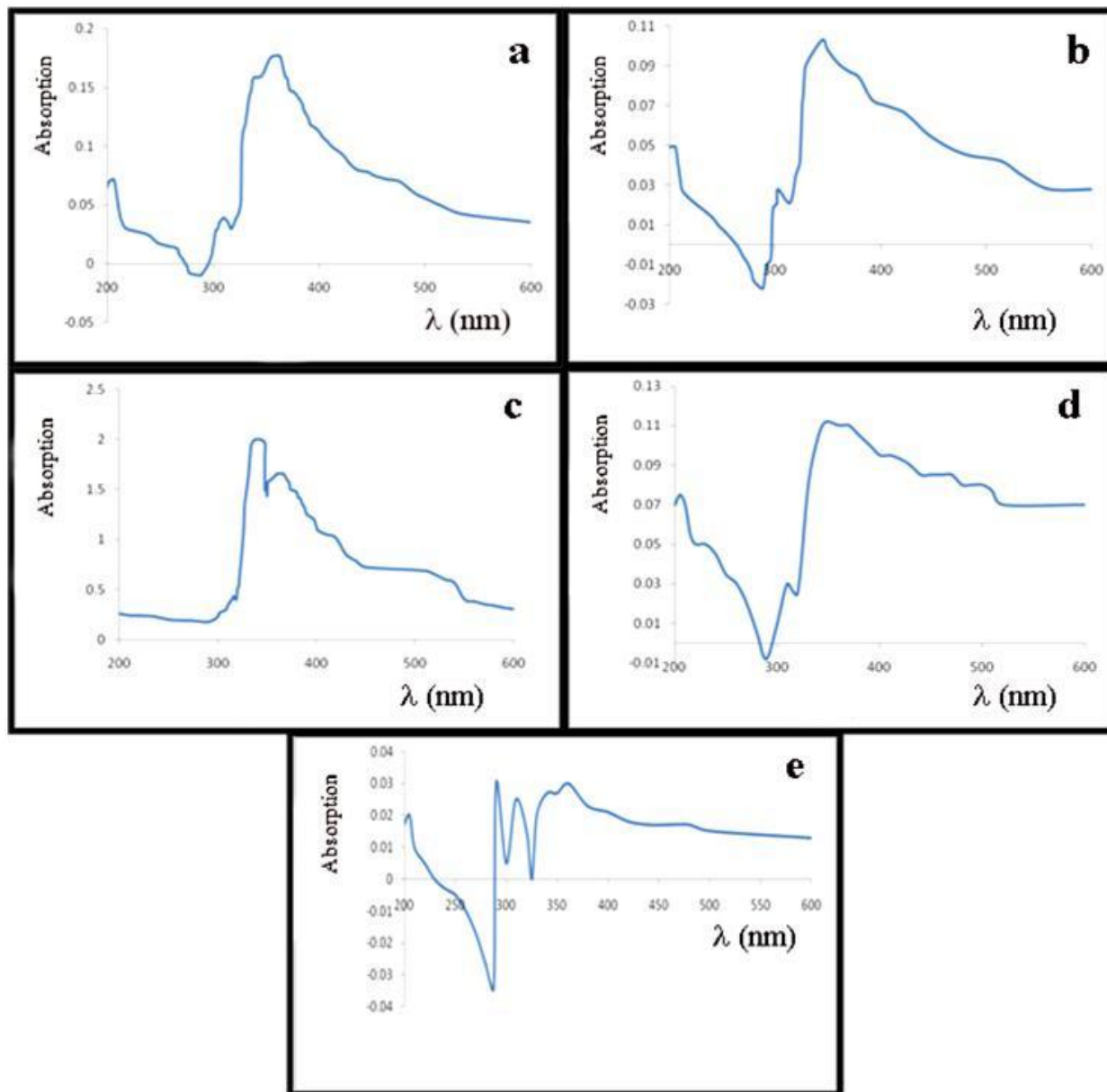


Figure 15. Uv-Visible range of five different experimental conditions of synthesis in the samples that are listed in Table 1.

Table 2. Effect of ZnO morphology on the λ_{max} and energy gap

Samples*	Morphology	Particle size (nm)	λ_{max} (nm)	Energy gap (eV)
a	Nanoparticles	30	362	3.43
b	Nanosheets*	30	344.5	3.61
c	Nanoparticles	50	363.5	3.41
d	Nanorods*	40	347.0	3.58
e	Nanoparticles	160	361.5	3.44

*a, b, c and d are the sample labels, according to Table 1. For nanosheets the noted size is for average thickness and about nanorods is for average diameter.

As it is obvious in Table 2, The sample morphology is the effective parameter can change the λ_{\max} as well as energy gap (compare the samples a, b and d) but, the ZnO particle size can not significantly change the energy gap (compare the samples a and e).

4. CONCLUSION

The results showed that a pulse galvanostatic method can be used as a of confidence and effective technique for the synthesis of various zinc oxide nanostructures by direct anodic oxidation of the zinc electrode in alkaline solution of sodium sulfide. Pulse and relaxation times, sodium sulfide and sulfate concentrations, height of pulse, temperature, mixing rate are effective parameters can vary morphology and particles size of the zinc oxide samples. By changing synthesis conditions, ZnO can be synthesized in different morphologies such nanosheet, nanorods and nanoparticles. The ZnO morphology can strongly change the sample energy gap.

ACKNOWLEDGEMENT

The authors would like to thank the financial support of this work by Abhar Payame Noor University Research Council

References

1. E. Manova, T. Tsoncheva, D. Paneva, I. Mitov, K. Tenchev, L. Petrov, *Appl. Catal. A*: 277 (2004) 119.
2. Mao-Sung Wu, Pin-Chi J. Chiang, Jyh-Tsung Lee, Jung-Cheng Lin, *J. Phys. Chem. B.*, 109 (2005) 23279.
3. L. Carbone, S. Kudera, E. Carlino, W. J. Parak, C. Giannini, R. Cingolani, L. Manna, *J. Am. Chem. Soc.*, 128 (2006) 748.
4. M. Regragui, M. Addou, A. Outzourhit, J. C. Bernede, E. E. Idrissi, E. Benseddik, A. Kachiuane, *Thin Solid Films*, 358 (2000) 40.
5. J. Xie, X. Cao, J. Li, H. Zhan, Y. Xia, Y. Zhou, *Ultrason. Sonochem.*, 12 (2005) 289.
6. Kh. Ghanbari, M. F. Mousavi, M. Shamsipur, *Electrochim. Acta*, 52 (2006) 1514.
7. M. Zhoua, S. Chena, S. Zhaoa, H. Ma, *Physica E.*, 33 (2006) 28.
8. A. Curulli, F. Valentini, S. Orlanducci, M. L. Terranova, C. Paoletti, G. Palleschi, *Sens. Actuators B.*, 100 (2004) 65.
9. O. Buriez, I. Kazmierski, J. Pe'richon, *Electroanal. Chem.*, 537 (2002) 119.
10. E. Perre, L. Nyholm, T. Gustafsson, P. L. Taberna, P. Simon, K. Edström, *Electrochem. Commun.*, 10 (2008) 1467.
11. S. C. Tang, X. K. Meng, S. Vongehr, *Electrochem. Commun.*, 11 (2009) 867.
12. H. Antonya, A. Labrit, J. C. Rouchaud, L. Legrand, A. Chausse, *Electrochim. Acta*, 53 (2008) 7173.
13. M. A. Del Valle, M. Gacitúa, F. R. Díaz, F. Armijo, R. del Río, *Electrochem. Commun.*, 11 (2009) 2117.

14. N. Cioffi, L. Torsi, L. Sabbatini P. G. Zambonin, T. Bleve-Zacheo, *Electroanal. Chem.*, 488 (2000) 42.
15. C. A. moina, M. Vazdar, *Electrochem. Commun.*, 3 (2001) 159.
16. P. Bocchetta, M. Santamaria, F. Di Quarto, *Electrochem. Commun.*, 9 (2007) 683.
17. M. Lai, D. Jason Riley, *J. Coll. Interface Sci.*, 323 (2008) 203.
18. S. Ghasemi, H. Karami, M. F. Mousavi, M Shamsipur, *Electrochem. Commun.*, 7 (2005) 1257.
19. L. M. Chang, M. Z. An, H. F. Guo, S. Y. Shi, *Appl. Surf. Sci.*, 253 (2006) 2132.
20. P. Gyftou, E. A. Pavlatou, N. Spyrellis, *Appl. Surf. Sci.*, 254 (2008) 5910.
21. N. S. Qu, K. C. Chan, D. Zhu, *Scripta Materialia.*, 50 (2004) 1131.
22. M. Ma, V. S. Donepudi, G. Sandib, Y. K. Sunc, J. Prakash, *Electrochim. Acta.*, 49 (2004) 4411.
23. H. H. Zhoua, S. Q. Jiaoa, J. H. Chenb, W. Z. Weib, Y. F. Kuanga , *Thin Solid Film.*, 450 (2004) 233.
24. H. Adelhani, M. Gaemi, *Solid State Ion.*, 179 (2008) 2278.
25. L. M. Chang, M. Z. An, H. F. Guo, S. Y. Shi, *Appl. Surf. Sci.*, 253 (2006) 2132.
26. P. Gyftou, E. A. Pavlatou, N. Spyrellis, *Appl. Surf. Sci.*, 254 (2008) 5910.
27. A. Khorsand Zak, W. H. abd. Majid, H.Z. Wang, R. Yousefi, A. Moradi Golsheikh, Z.F. Ren, *Ultrason. Sonochem.*, 20 (2013) 395.
28. P. Rai, W. Kwak, Y. Yu, *ACS Appl. Mater. Interfaces*, 5 (8) (2013) 3026.
29. B. Liu, H. Zeng, *J. Am. Chem. Soc.*, 125 (15) (2003) 4430.
30. X. Y. Kong, Z. L. Wang, *Nano. Lett.*, 3 (2003) 1625.
31. B. D. Yao, Y. F. Chan, N. Wang, *Appl. Phys. Lett.*, 81 (2002) 757.
32. H. Karami, *Int. J. Electrochem. Sci.*, 5 (2010) 720
33. D. Costenaro, F. Carniato, G. Gatti, L. Marchese, C. Bisio, *New J. Chem.*, 37 (2013) 2103.
34. H. F. Lin, S. C. Liao, S. W. Hung, *J. Photochem. Photobiol. A.*, 174 (2005) 82.